Research Article

Petrochemical constrains on the origin and tectonic setting of mafic to intermediate dykes from Tikar plain, Central Cameroon Shear Zone

Benjamin Ntieche[1] · M. Ram Mohan[2] · Amidou Moundi[3] · Pauline Wokwenmendam Nguet[4] · Mahomed Aziz Mounjouohou[5] · Zakari Nchouwet[3] · Daouda Mfepat[3]

Received: 31 August 2020 / Accepted: 20 January 2021 / Published online: 25 January 2021

Abstract

The Tikar plain is located on the Cameroon Central Shear Zone. It is also part of the North Equatorial Pan-African Belt. It is formed of granitoids intruded in places by mafic and intermediate dykes. The mafic dykes are essentially banded gabbros composed of plagioclases, pyroxenes, amphiboles, biotites and opaques. Their textures range from porphyroblastic to porphyritic. The intermediate dykes are monzonites and monzodiorites and are characterized, respectively, by cataclastic and mylonitic textures. The minerals identified are amphiboles, potassium feldspar, pyroxenes, epidotes, sphenes and opaques. Seritization reaction is mostly present on the mafic and intermediate dykes, while chloritization is much more pronounced on the intermediate dykes. The Tikar plain dykes are high-k calc-alkaline to shoshonitic. They are characterized by low to moderate SiO_2 content (42.08–61.96 wt%), low to high TiO_2 (0.47–2 wt%) and low Ni (1.48–99.18 ppm) contents. The mafic dykes show fractional trends with negative anomalies of Zr, U and P and positive Rb, Ba, Ta, Pb and Sr in multi-element diagrams, while the intermediate dykes present negative anomalies of Nb, Ta, Zr, Sr P and Ti and relative positive anomalies of Rb, Ba and Pb. The rare-earth elements (REE) patterns show positive Eu anomalies for the mafic dykes and negative anomalies for the intermediate dykes. The REE spectrum of all the dykes shows enrichment in LREE with relatively flat HREE, which can indicate arc magmatism. In the Zr–Ti/100–Sr/2 diagram, the mafic dykes plot in the island arc tholeiite and calc-alkaline basalt fields. The Th, Nb and LREE concentrations indicate that the subducted lithosphere with crustal component contributed to generation of the intermediate dykes of the Tikar plain. The geochemical characteristics of the mafic to intermediate dykes suggest their derivation from a various degree of partial melting in the garnet spinel facies, probably between depths of 80 and 100 km. The collision between the Central African Fold Belt and the northern edge of the Congo craton resulting in crustal thickening, sub-crustal lithospheric delamination and upwelling of the asthenosphere may have been the principal process in the generation of the intermediate dykes in the Tikar plain. The magma for the mafic and intermediate dyke would have migrated through the faults network of the Central Cameroon Shear Zone before crystallizing in the granito-gneissic basement rocks.

Keywords Dykes · Tikar plain · Collision · Shear · Delamination

✉ Benjamin Ntieche, ntiechebenjo@yahoo.fr | [1]Geology Laboratory, Higher Teacher Training College, University of Yaounde 1, P.O. Box 47, Yaounde, Cameroon. [2]CSIR-National Geophysical Research Institute, Hyderabad-500 007, India. [3]Department of Earth Sciences, University of Yaounde 1, P.O. Box 812, Yaounde, Cameroon. [4] Institute of Geological and Mining Research, P.O. Box 4110, Yaounde, Cameroon. [5]Department of Earth Sciences, University of Maroua, P.O. Box 814, Maroua, Cameroon.

SN Applied Sciences (2021) 3:211 | https://doi.org/10.1007/s42452-021-04265-5

1 Introduction

Precambrian rocks in Cameroon are divided into two lithotectonic groups, namely the Ntem group and the Pan-African North Equatorial Folded Belt (PANEFB) [1–3]. Located in southern Cameroon, the Ntem group is made up of the Ntem Archean unit and the Ayna and Nyong Paleoproterozoic units, while the North Equatorial Pan-African belt dated 0.6 Ga [4, 5] occupies the northern part of the country. PANEFB in Cameroon is characterized by thrusting and transcurrent tectonics [6, 7] which favored the formation of the N–S to ENE–WSW oriented shears along the Adamawa Shear Zone (ASZ) (Fig. 1). PANEFB evolutionary geotectonic models in Cameroon show an early extension that led to the formation of Early Neoproterozoic sedimentary basins followed by subduction and collision between the Saharan metacraton and the Congo craton at 0.6 Ga [8]. In Cameroon, this extensive tectonic regime led to the formation of intracratonic basins or graben covered with Cretaceous sedimentary deposits, accompanied by Mesozoic to Lower Cenozoic magmatism that favored the formation of granitic or gabbroic plutons and some dykes swams and volcanic deposits [9]. Graben dykes have been extensively studied in the PANEFB in Cameroon, but the dykes from the Tikar plain (mafic to intermediate dykes) located in the central corridor of the Foumban–Banyo Shear Zone remain unstudied. Owing the fact that the mafic to intermediate dykes are of great interest for the understanding of the tectonic evolution of a given area, we present in this article, the field, petrographic and whole rock geochemical data of mafic to intermediate dykes of the Tikar plain and discuss the petrogenesis, magmatic evolution, mantle source as well as the tectonic settings of the dykes in order to deduce the tectonic evolution of the Tikar plain in particular and PANEFB in Cameroon in general.

2 Regional geological framework

The Tikar Plain is located on the Central Shear Zone of Cameroon (CCSZ) which is a unit of the North Equatorial Pan-African belt in Cameroon. This Pan-African chain is made up of three major lithological and tectonic domains, namely the Northwestern Cameroon (NWCD) domain, the Adamawa Yade domain (AYD) and the Yaoundé domain (YD) (Fig. 1).

The Northwestern Cameroon Domain (NWCD), also called the Poli group [11, 12], is located in the northern part of Cameroon and is limited to its southern part by the Tchollire Banyo (TBF) fault. It hosts meso- to neo-proterozoic volcano-sedimentary basins that have been variably metamorphosed into schists and gneisses [13]. The NWCD is covered with locally metamorphosed detrital and volcanic deposits and pre-, syn- or late-tectonic calc-alkaline intrusions (diorites, granodiorites and granites) [12, 14, 15].

The Adamawa Yade domain to which belongs the study area is limited in its northern part by the Tchollire-Banyo Fault (TBF) and in the south by the Sanaga Fault (SF)

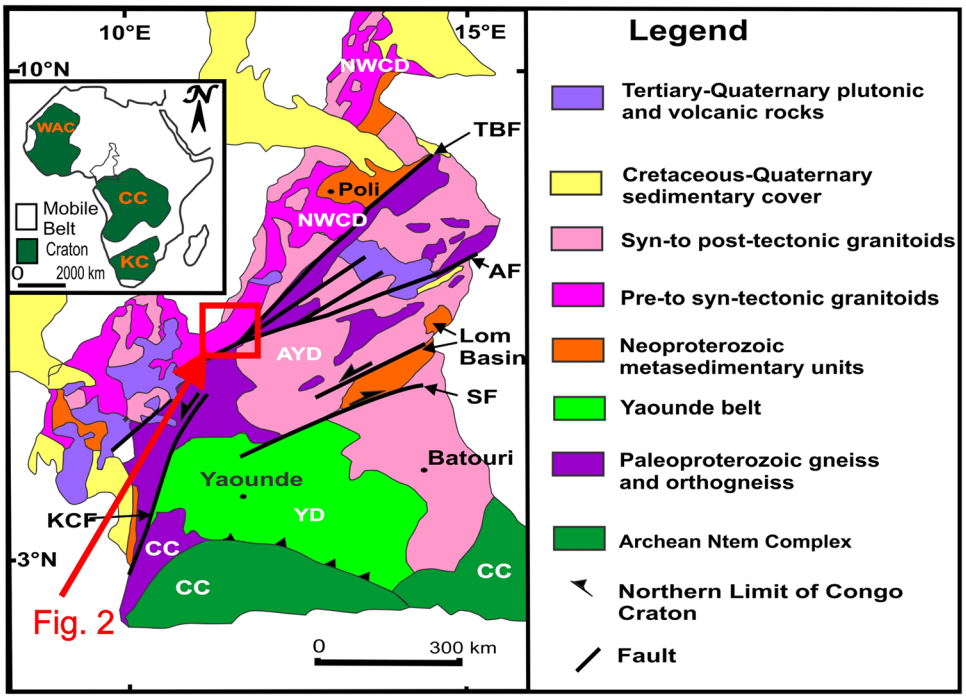

Fig. 1 Geological map of Cameroon modified after [10]. Fault system comprises the Tchollire–Banyo Fault (TBF), the Adamawa Fault (AF), the Sanaga Fault (SF) and the Kribi–Campo Fault (KCF). The insert is the map of the African continent, showing the location of Cameroon and the distribution of cratons and mobile belts (*WAC* West African Craton, *CC* Congo Craton, *KC* Kalahari Craton)

(Fig. 1). It hosts large Pan-African intrusions and Paleoproterozoic relics metamorphosed and settled during Pan-African tectonic evolution.

The Yaoundé domain located to the south of Cameroun is limited in its northern part by the Sanaga fault and to the south by the Congo craton. It is formed by metasediments and pre- to syn-tectonic rocks with alkaline and transitional affinities [13]. In its southern part, we note the predominance of gabbros, diorites, mafic dyke outcrops and/or serpentinized ultramafic rocks [16].

Located in the western part of the Adamawa Yade domain (Fig. 2), the Tikar Plain is mainly made up of pan-African granitoids [10, 17] (Fig. 1). Chemically, the granitoids of the Tikar Plain are subdivided into diorites, granodiorites and granites [18, 19]. The basement rocks consist of Paleoproterozoic gneisses and amphibolites of meta-igneous and meta-sedimentary origin [17, 18]. The granitoids of the Adamawa–Yade domain are classified as syn-, late and post-tectonic [10, 18–20]. Structurally, the basement rocks of the Adamawa Yade domain has undergone four phases of deformation (D1 to D4); each phase being characterized by plane linear and plano-linear structures [20, 21]. The granitoids emplacement has been favored by the replay of the Central Cameroon Shear Zone [22–25]. The granitoids from the Tikar Plain are associated in places to few mafic to intermediate dykes outcrops [20] (Fig. 3) that are not yet been studied in detail.

3 Methodology

A total of thirty (30) rock samples were taken during the fieldwork. Geochemical analyses were carried out at the laboratory of the CSIR-National Geophysical Research Institute (NGRI), Hyderabad, India. The analytical method used in this work is widely explained in [27].

For the geochemical analyses of major and trace elements, 20 samples selected free from alterations were selected. The samples were then crushed and then pulverized.

Preparation of sample powders and reference materials for analysis of major elements required 2 g of finely ground sample (– 200 mesh ASTM) or standard filled in aluminum cups [28]. Then, about 2.5 g of boric acid was added, and then, these cups were put under hydraulic pressure to obtain the pellet. The major elements were analyzed in a Phillips® MagiX PRO Model 2440 X-ray Fluorescence Spectrometer (XRF) (Philips, Eindhoven), and calibration graphs were obtained using SUPER Q 3.0 analytical software.

To prepare the curves, international reference materials on rocks from USGS, National Institute of Geophysical Research of India, Geological Survey of Japan, Natural Resources Canada and International Working Groups (France) have been used. The accuracy and precision of the analysis was 2% RSD for almost all major elements.

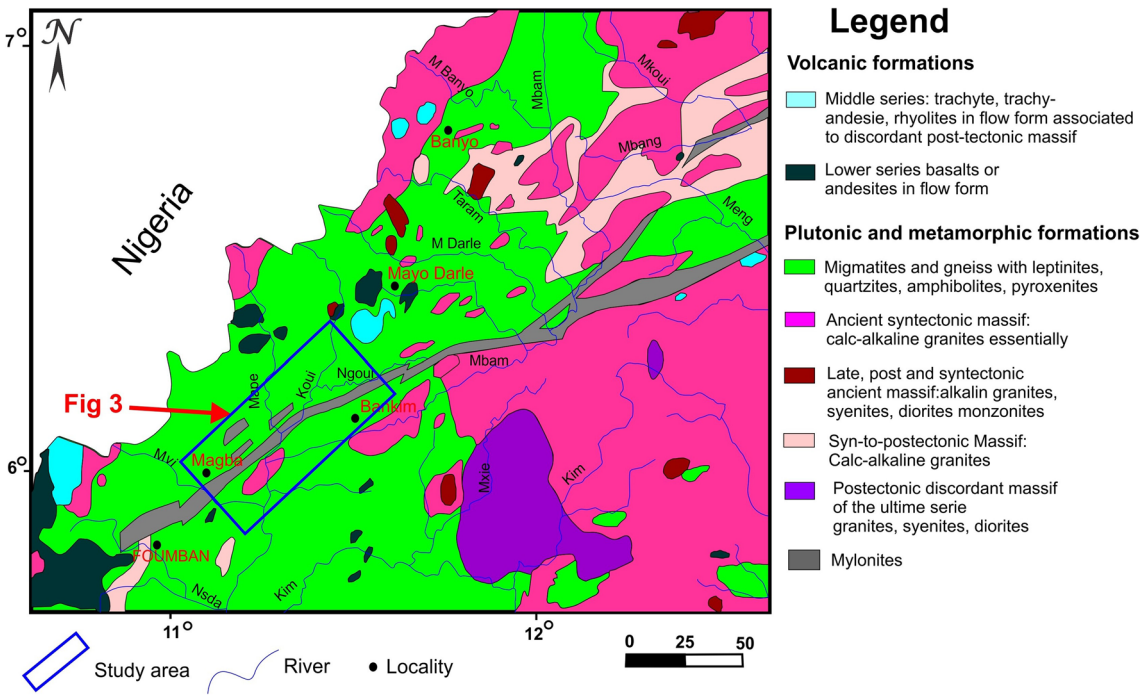

Fig. 2 Geological map of the western Adamawa Yade domain [26]

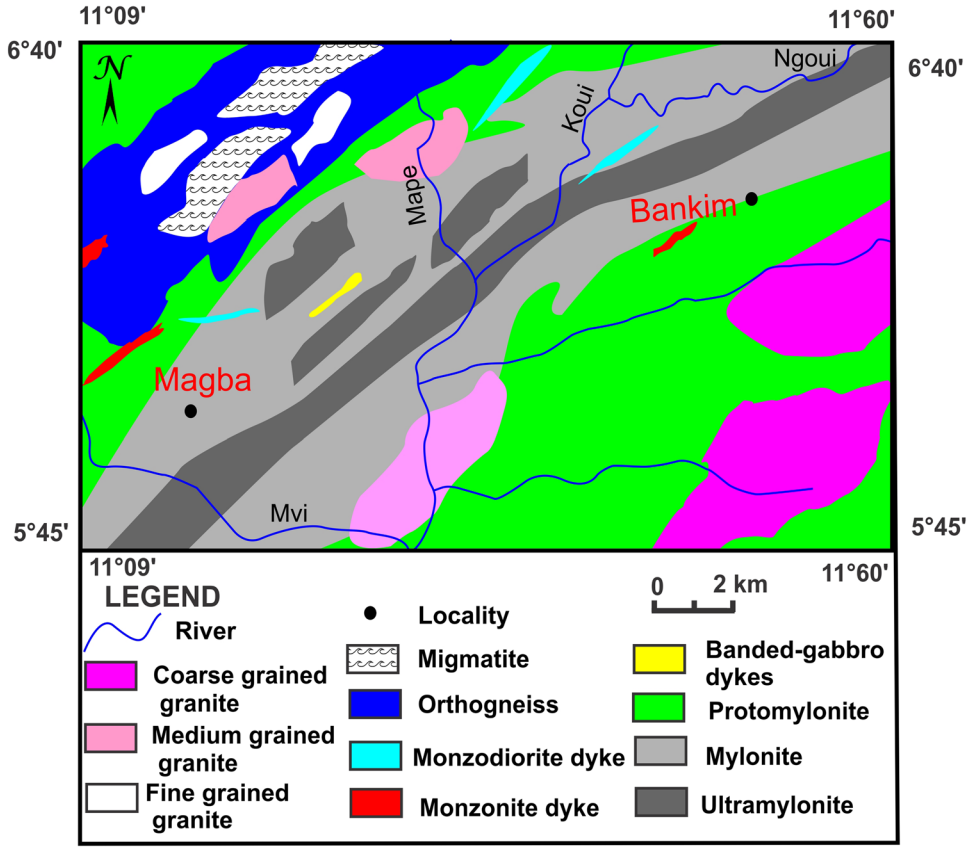

Fig. 3 Geological sketch map of the Tikar plain

For the trace elements analysis, 0.05 g of sample was introduced into 25 ml of Teflon Savillex pressure decomposition vessels. An acid mixture (HF:HNO_3) was used to dissolve the homogenized powder sample in Savillex® screw containers, and 10 ml of an acid mixture (containing 7:3:2 HF–HNO_3–HCl) was added to each sample. Then, 5 ml of a 1 ng/ml solution of 103Rh was added to each Savillex vessel as an internal standard. After homogenization of the mixture, the containers were sealed and stored on a hotplate at ~ 140 °C for 48 h. After that, the containers were opened and the contents were heated until evaporation at 200 °C; then, a few drops of $HClO_4$ were added to ensure the complete removal of HCl and HF from the mixture. After obtaining the residue, 10 ml of 1: 1 HNO_3 was added and the volume was brought to 250 ml with Milli Q® deionized water (18 MQ). Finally, the solution was stored in HDPE bottles. The certified reference materials, namely JG-2, JG-3, JB-2 from the Geological Survey of Japan and G-1A, G-2 from the USGS as well as the procedure blanks were prepared with the batch of samples using the same protocol described above. The very clear solutions obtained for all samples and standards were analyzed using the PerkinElmer® model ELAN® DRC ™ II mass spectrometer (PerkinElmer, Inc., Shelton, CT, USA) at the CSIR-National Geophysical Research Institute laboratory (NGRI), Hyderabad. An internal standard used was 103Rh, and external errors were corrected by repeated analyses of a 1: 5000 solution of the JG-2, JG-3 and JB-2 standards.

The primitive mantle normalization values for the multi-element diagram and the REEs are from [29].

4 Results

4.1 Field relationship

The outcrops of mafic and intermediate dykes intrude granites, gneisses and migmatites (Fig. 3). Banded-gabbros outcrops are exposed in the form of dykes or slabs. They are dark green in color and broadly banded. The banding is marked by large subvertical dark bands formed of mafic minerals (biotite, amphibole and pyroxene) and the thin clear bands formed of quartzo-feldspathic minerals (mostly feldspar) (Fig. 4a). In places, the rock is intersected by few quartzo-feldspathic veins of centimeter thickness more or less parallel to the foliation direction NE-SW. Some minerals like feldspar are stretched and elongated in the same NE-SW direction. The contact between banded gabbros and gneiss is sharp indicating that they are not coeval.

The monzodiorites occur in the form of dark dykes in the Mape dam and Badam hill (Fig. 4b). At the Mape dam, they are exposed in the form of intrusions of about

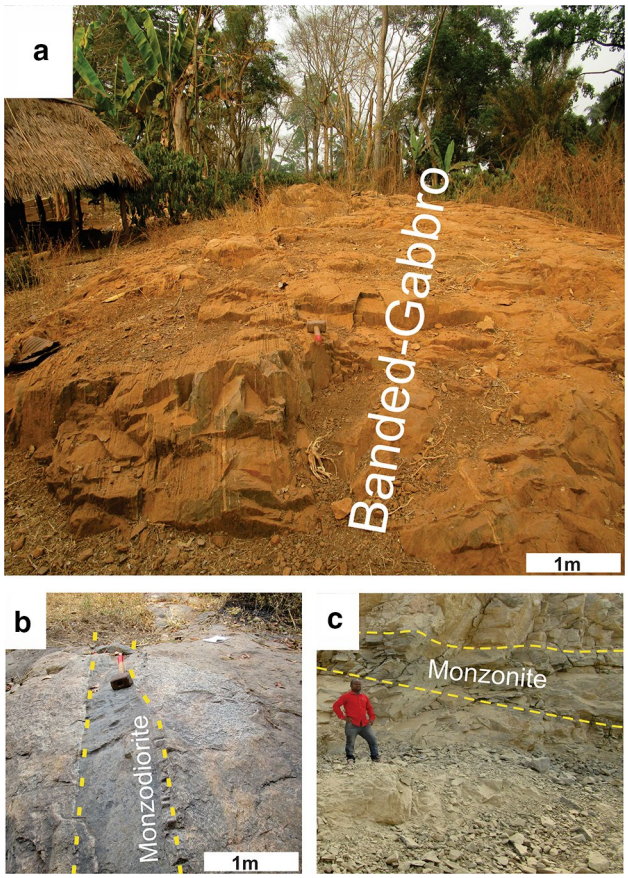

Fig. 4 Field photographs of the dykes. **a** Banded-gabbro dyke with vertical foliation. Note the thin quartzo-feldspathic bands alternating with large ferromagnesian layers, **b** monzodiorite intruding fine grain granites in Bankim, **c** monzonite outcrop intruding granite in Magba

5–30 cm wide and 2–15 m length and stretched in the NE–SW direction. The rock is more or less crushed and sometimes associated with migmatites and orthogneiss. The monzonites have a thickness of about 2–5 m, and their length ranges from 5 to 20 m. In places, they are fractured, following the NW–SE and NE–SW directions.

The monzonites are exposed in the Magba, Mape, Mbakop, Nkoula and Nyakon areas. They are mostly aphyritic (Fig. 4c) and are particularly exposed at the slopes and hill tops in the form of dykes or slabs. In places, the rocks are foliated. Feldspar and quartz are more or less visible in size and preferably oriented. Some deformation marks and kinematics indicators are observed on certain monzonites outcrops. These indicators are feldspar grains in the form of sigma "σ" and delta "θ" (monzonites from Mfendagnam and Nyakon), shear and joints.

4.2 Petrography

4.2.1 Banded gabbros

The banded gabbros have porphyroblastic texture (Fig. 5a). It consists of plagioclase (20–45%), pyroxene (10–20%), amphibole(8–12%) and biotite (5–15%) as principal minerals, while chlorite (5–10%) and sericite (2–5%) are the secondary mineral and opaques (1–2%) the accessory phase. The most represented minerals are plagioclase. They are in the form of euhedral and subhedral macro- and micro-crystals. Some crystals have well-marked polysynthetic twins with biotite inclusions in places. Sericitization reactions are also present on some plagioclase slats. Sericite presents a dusty or powder form (Fig. 5a) and fills the minerals cracks and interstices. Pyroxene is present in the form of sub-euhedral grains. It is most commonly associated with amphibole and biotite. In places, it occurs as inclusions in plagioclase phenocrysts along with biotite. Some few crystals present simple twinning. The amphiboles also display simple twins and are associated with biotite. Amphibole and biotite flakes are in places altered to chlorite.

4.2.2 Monzodiorites

Monzodiorites have varying textures. The most representative are the fine grained, porphyritic, porphyroblastic, mylonitic and cataclastic textures (Fig. 5b–d). They consist of potassium feldspar, quartz, amphibole, pyroxene, biotite, chlorites, titanites, epidote and opaques. K-feldspar crystals (20–40%) are abundant and some crystals show deformation marks such as fractures and shears. In places, K-feldspar porphyroblasts appear in the form of sigma "σ" or delta "θ" (Fig. 5c), indicating that the rock has undergone a shearing deformation in the dextral or sinistral direction. They are sometimes associated with amphiboles (20–30%). Amphibole crystals are subhedral and occur in places with fish shape "amphibole fish," attesting that the monzodiorites have undergone deformation (Fig. 5b). Some crystals have undergone the chloritization reaction. Quartz crystals (10–25%) are abundant and appear in the form of isolated crystals or polycrystalline ribbon. Pyroxene (10–15%) is rare and even absent in some samples. It is subhedral to anhedral and associated with the amphibole and biotite. Chlorite (2–5%) is the alteration product of amphiboles and biotites, and they occur at the edge of the amphiboles or pyroxenes. Epidote (2–3%) is mostly euhedral and is located in the micro-fractures traversing the rock. They are found in places associated with opaques and titanites.

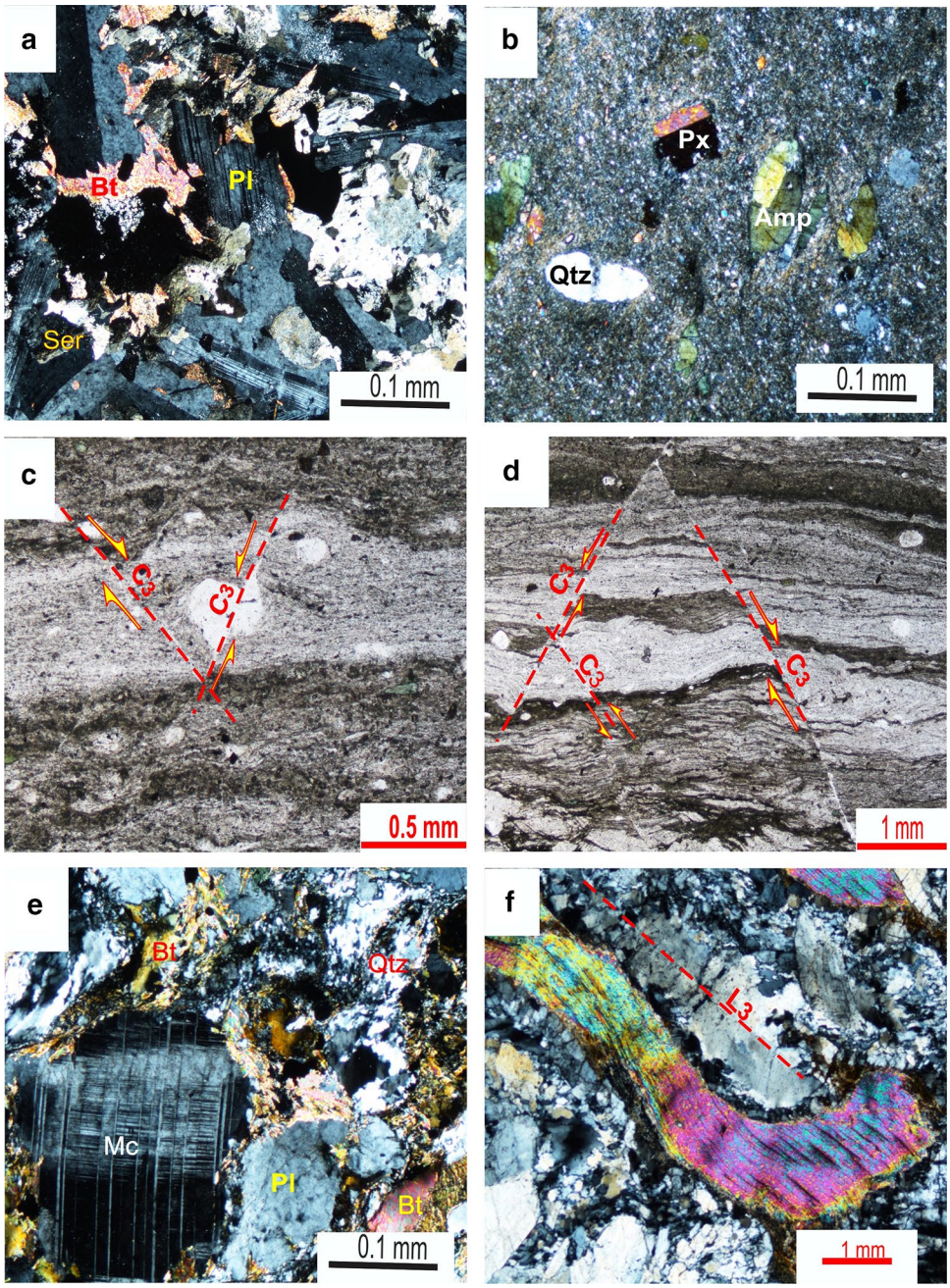

Fig. 5 Microphotographs of rock textures, mineral reactions and deformation (**a**, **b**, **e** and **f** are crossed polarized light images, **c** and **d** are plane polarized light images). **a** Porphyritic texture on banded-gabbro. Note the sericitization reaction on the plagioclase minerals, **b** cataclastic texture in mozodiorite. Note the fish shape of the amphibole and pyroxene disseminated in the rock, **c**–**d** mylonitic texture on monzodiorite marked by the alternation of mafic and quartzo-feldspathic bands. Note the deformation features highlighted by the dextral shear C_3 on the sigma feldspar porphyroblast "σ" and the sinistal and dextral shear C_3 on the bands, **e** granoblastic texture on the monzonite. Note the plagioclase porphyroblast molded by biotite flakes. **f** Curved biotite flake elongated along lineation line L_3 and surrounded by aligned feldspar and recrystallized quartz sub-grains (*Qtz* quartz, *Pl* plagioclase, *Px* pyroxene, *Amp* amphibole, *Bt* biotite, *Mc* Microcline, *Ser* sericite)

4.2.3 Monzonites

The textures that characterize the monzonites are porhyritic and granoblastic (Fig. 5e). The most common mineral here is quartz (30–40%). It is xenomorphic and occurs under two generations, namely monocrystalline and polycrystalline. Monocrystalline quartz is subhedral and is associated with alkali feldspars and plagioclase. Polycrystalline ribbon quartz presents flaky form or appears in place in the form sands (Fig. 5e, f) molding the feldspar minerals and monocrystalline quartz. They also fill minerals interstices along with sericite, chlorite or epidote. Plagioclase (10–30%) and orthoclase (5–15%) are the most represented feldspars. In some places, the plagioclase has undergone either saussuritization or sericitization reaction, while orthoclase is transformed into microcline. Biotite (5–15%), pyroxene (2–5%) and amphibole (8–10%) are the most common ferromagnesians in the rock. They are altered to chlorite (1–5%) which fills the interstices of the minerals together with sphene (1–2%), epidote (1–5%) and stream quartz. In places, the biotite is stretched according to the mineral lineation (Fig. 5f), demonstrating that the rock has experienced deformation.

4.2.4 Geochemistry

The geochemistry of major and trace elements, including rare-earth elements, was done on rock samples selected based on their freshness and their representativeness. The data presented in Table 1 were used for the classification of the rocks, their geochemical, petrogenetic and geotectonic analyses.

According to the TAS classification diagram of [30], the mafic dykes studied are classified as gabbros, and the intermediate dykes are classified as monzodiorites and monzonites (Fig. 6a).

In the Co–Th diagram of [31] (Fig. 6b), the mafic and intermediate dykes are high-k calc-alkaline and shoshonitic in composition. All the studied dyke samples fall within the calc-alkaline series (Fig. 6c) on the AFM diagram [32]. According to the Na_2O–K_2O–Al_2O_3 triangular diagram (Fig. 6d), the studied dykes show metaluminous character. The LOI contents of the samples vary from 0.21 to 1.58 wt.%, indicating that the selected rock samples are not significantly altered [33].

4.2.5 Banded-gabbro

The banded-gabbro has SiO_2 contents ranging from 47.08 to 48.61 wt%. The MgO varies from 9.12 to 9.43 wt%, the CaO from 9.01 to 9.89 wt% and the LOI from 0.81 to 1.58. The TiO_2 contents (0.99–1.07 wt%) are moderate. The concentrations of Ni (28.82–99.18 ppm) and Cr (120–126 ppm) are lower than those of rocks originating from a partial melting of the mantle (Ni > 200 ppm and Cr > 400 ppm). The primitive mantle normalized diagram [29] of the banded gabbros is marked by an enrichment in Rb, Ba, Ta, Pb and Sr and a relative depletion in U, Zr and Ti (Fig. 7a). The primitive mantle normalized REE diagram [29] (Fig. 7b) is slightly enriched in LREE (La_N/Sm_N = 1.69–2.15) compared to HREE and displays positive europium anomalies (Eu/Eu* = 1.24–1.34). The spectrum shows a weak fractionation of the LREE ((La/Yb) cn = 3.48–4.74) with the relatively flat curve of the HREE in the form of a flattened hyperbola.

4.2.6 Monzodiorite

The monzodiorite has a moderate SiO_2 contents ranging from 52.07 to 55.38 wt%, high TiO_2 (1.56–2 wt%) and K_2O (2.66–4.11 wt%) contents and moderate CaO (7.77–9.06 wt%) and Al_2O_3 (11.42–13.78 wt%) contents. The Fe_2O_3 (4.34–10.5 wt%) and MgO (4.87–8.94 wt%) concentrations are low to high. The LOI contents vary from 0.35 to 0.47 wt%. The high TiO_2 contents attest to the presence of titanite in thin section. The molecular ratio Al_2O_3/ ($CaO + Na_2O + K_2O$) of the monzodiorite varies from 0.68 to 0.93 and confirms their metaluminous character.

The samples show low to high contents of Co (14.37–29.42 ppm), Sc (14.35–21.15 ppm) and Cr (15.97–82.36 ppm), moderate contents of Y (74.62–89.19 ppm) and low Zr contents (166.83–312.39 ppm). The primitive mantle normalized diagram [29] of the samples shows a slight enrichment of Rb and Th, but pronounced depletions in Sr, Zr and Ti (Fig. 7c). In the REE diagram [29] (Fig. 7d), the monzodiorites show enrichments in LREE (La_N/Sm_N: 1.97–2.81) with relatively flat HREEs and negative europium anomalies (Eu/Eu* = 0.60–0.75).

4.2.7 Monzonites

The monzonites have moderate to high SiO_2 contents (53.71–61.96 wt%). The concentrations of TiO_2 (0.47–1.75 wt%), CaO (2.90–11.4 wt%) and K_2O (3.05–5.97 wt%) are low to high, whereas those of Al_2O_3 are moderate to high (11.54–17.23 wt%). The monzonites have LOI values varying from 0.21 to 1.58 wt%. They have low to high contents of Th (2.04–16.01 ppm), Cr (11.39–451.52 ppm) and Zr (38.23–436.47 ppm) and low contents of Sc (3.65–14.85 ppm) and Y (13.11–32.48 ppm). The normalization diagram [29] of the samples shows enrichment in Rb, Ba and Pb and depletion in Nb and Ti (Fig. 7e).

The primitive mantle normalized REE diagram [29] (Fig. 7f) of the monzonites shows enrichment in LREE (La_N/Sm_N = 2.72–5.64) and depletion in HREE marked by a relatively flat HREE spectrum and a negative europium anomaly (Eu/Eu*: 0.74–0.99).

5 Discussion

5.1 Crustal contamination

The study of crustal contamination is very important while discussing the petrogenesis of mafic igneous rocks [34–36]. Thus, the possibility of contamination of mafic to intermediate dyke samples from the Tikar Plain area is discussed here on the basis of their geochemical characteristics.

It has been shown that the behaviors of certain trace elements (such as Sr, Zr and Nb) are used successfully in the verification of the involvement of crustal contamination during the formation of igneous rocks [37–41]. Mafic igneous rocks contaminated by the crust generally show significant negative Nb and Zr anomalies and positive Sr anomaly on the multi-element diagrams [37–41]. It has

Table 1 Major (wt%) and trace (ppm) element contents in mafic and intermediate dykes

Rock type	Banded-gabbro		Monzodiorite			Monzonites								
Sample no	PT12A	MGB	PT12	PT1	PT9	PTB3	PTB1	PTB6	PTB	PT11	PTK3	PTS1	PTBN3	PTD3
SiO_2	48.61	47.08	52.07	55.38	53.03	58.77	58.74	61.96	53.71	58.45	59.12	60.00	60.63	60.92
TiO_2	0.99	1.07	2	1.91	1.56	1.18	1.03	0.51	1	0.47	1.04	1.75	1.64	0.68
Al_2O_3	15.28	16.52	11.76	13.78	11.42	12.47	11.59	13.36	13.29	11.95	14.55	12.59	11.54	17.23
Fe_2O_3	10.55	10.57	10.5	4.34	8.06	5.99	5.80	5.99	5.84	3.9	4.38	6.59	7.64	5.04
MnO	0.14	0.11	0.17	0.17	0.15	0.10	0.09	0.09	0.1	0.06	0.08	0.09	0.09	0.07
MgO	9.12	9.43	4.87	8.44	8.94	7.07	7.96	5.12	5.59	4.67	7.83	5.90	5.33	3.67
CaO	9.89	9.01	9.06	7.77	8.19	4.60	4.69	5.33	9.98	11.4	5.54	4.50	4.70	2.90
K_2O	1.31	1.60	4.11	2.74	2.66	5.97	4.85	3.05	4.61	3.07	3.40	5.82	4.47	4.10
Na_2O	2.86	2.03	4.03	4.27	4.48	3.23	3.84	3.99	3.8	4.45	4.09	3.13	2.87	3.92
P_2O_5	0.15	0.18	0.84	0.36	0.64	0.43	0.41	0.18	0.43	0.17	0.27	0.50	0.60	0.20
LOI	0.81	1.58	0.47	0.37	0.35	0.83	0.52	0.25	0.50	0.21	0.35	0.65	1.58	1.03
Total	99.71	99.18	99.88	99.53	99.48	100.64	99.52	99.83	98.85	98.80	100.65	101.52	101.09	99.76
Sc	33.89	26.23	21.15	18.97	14.36	9.08	3.66	8.43	14.85	9.44	12.36	10.87	13.81	9.53
V	176	150	45.32	211	44.47	28.54	15.94	30.82	85.80	69.71	115	614	747	68.95
Cr	120.10	126.11	74.11	82.36	15.97	11.93	12.17	16.24	48.51	70.29	61.56	371	451	166
Co	59.31	44.47	29.42	18.81	14.37	9.96	5.80	9.99	16.99	16.14	18.80	16.70	18.66	12.21
Ni	28.89	99.18	21.42	1.95	2.42	2.33	1.48	1.954	13.40	11.40	14.01	8.39	8.64	61.56
Cu	101.65	77.09	92.41	0.68	0.40	0.15	0.14	0.263	30.25	144	51.80	44.75	51.92	57.66
Zn	74.62	57.18	121.74	39.34	30.08	25.30	14.47	18.30	77.41	60.07	85.73	117.36	116.60	55.72
Ga	18.62	13.55	32.96	28.90	28.47	26.54	21.64	18.28	29.14	21.01	26.89	26.35	29.97	17.50
Rb	36.30	27.50	66.30	120	125	226	134	81	203	93	93	190	229	99
Sr	775	528	453	393	546	997	676	581	1361	669	850	547	608	517
Y	19.07	18.58	87.96	89.19	74.62	31.85	13.50	13.11	32.48	13.24	30.08	29.11	26.11	20.95
Zr	94.16	46.38	193	312	166	436	255	65	321	88.87	38.23	93.19	131	74.28
Nb	4.23	12.13	26.59	47.50	27.40	18.41	7.99	6.56	11.23	3.64	5.74	16.35	13.48	15.21
Cs	0.40	0.24	1.51	8.11	4.05	8.34	2.21	1.56	9.02	5.86	2.62	5.09	2.62	1.86
Ba	242	235	1346	251	299	1693	666	977	1714	1193	1010	1193	1214	1103
Hf	2.14	1.38	3.93	11.32	5.97	13.60	8.38	2.57	7.20	2.29	0.94	2.34	2.96	2.19
Ta	0.52	4.21	3.40	4.08	4.08	0.76	0.30	0.21	2.52	0.78	0.74	1.59	3.18	6.10
Pb	5.41	5.05	43.39	77.46	24.44	26.08	26.09	29.98	4.66	8.01	4.23	14.98	5.64	15.60
Th	0.50	0.85	12.39	17.98	13.30	16.01	15.20	3.32	5.06	2.39	2.04	3.89	10.22	12.01
U	0.04	0.13	7.77	11.43	3.50	4.50	5.53	1.18	0.46	0.37	0.89	0.37	0.72	1.34
La	8.48	11.01	64.80	73.28	90.81	99.01	52.79	20.53	66.05	20.38	54.56	50.59	72.58	50.04
Ce	20.14	23.06	166	189	213	207	97.60	42.96	149	43.75	100	116	166	89.68
Pr	2.38	2.76	19.04	25.24	26.25	22.52	10.02	5.13	15.61	4.54	10.81	12.52	17.40	8.89
Nd	13.67	11.92	104	108	107	87.66	37.80	21.71	79.50	22.83	52.09	64.88	85.30	32.40
Sm	3.14	3.19	20.62	20.50	20.21	14.03	5.85	4.16	13.97	4.08	8.46	11.64	13.25	6.38
Eu	1.48	1.29	4.11	4.08	3.12	2.52	1.11	0.83	3.33	1.20	2.05	2.52	2.67	1.43
Gd	3.54	3.09	18.83	13.50	12.47	7.58	3.18	2.64	10.29	3.3	6.84	9.13	9.05	4.61
Tb	0.56	0.46	2.79	2.13	1.915	0.99	0.41	0.36	1.22	0.44	0.89	1.16	1.05	0.56
Dy	3.13	3.11	14.39	13.98	11.99	5.63	2.36	2.33	5.54	2.11	4.45	5.25	4.55	3.33
Ho	0.63	0.59	2.85	2.78	2.33	1.01	0.43	0.44	0.97	0.40	0.84	0.92	0.79	0.61
Er	1.89	1.60	8.39	7.15	5.93	2.49	1.07	1.11	2.85	1.17	2.56	2.49	2.24	1.67
Tm	0.32	0.24	1.25	0.96	0.79	0.31	0.13	0.14	0.44	0.19	0.38	0.36	0.33	0.25
Yb	1.69	1.61	6.95	6.80	5.52	2.13	0.94	1.01	2.61	1.09	2.18	1.96	1.84	1.68
Lu	0.26	0.23	0.98	0.99	0.80	0.31	0.13	0.14	0.39	0.16	0.31	0.27	0.26	0.24
Sum REE	61.28	64.17	435	469	503	453	213	103	352	105	246	280	378	201
Sr/Y	40.69	28.44	5.16	4.41	7.32	31.31	50.07	44.34	41.91	50.54	28.26	18.80	23.29	24.69

Table 1 (continued)

Rock type	Banded-gabbro		Monzodiorite			Monzonites								
Sample no	PT12A	MGB	PT12	PT1	PT9	PTB3	PTB1	PTB6	PTB	PT11	PTK3	PTS1	PTBN3	PTD3
(Eu/Eu*)N	1.34	1.24	0.64	0.75	0.60	0.74	0.78	0.76	0.84	0.99	0.82	0.74	0.74	0.80
(La/Yb)N	3.48	4.74	6.47	7.47	11.41	32.17	38.96	14.00	17.49	12.86	17.35	17.90	27.27	20.62
(La/Sm)N	1.69	2.15	1.97	2.24	2.81	4.41	5.64	3.08	2.96	3.12	4.03	2.72	3.42	4.90
A/CNK	1.09	4.54	0.68	0.93	0.74	0.90	0.87	1.08	0.72	0.63	1.12	0.94	0.96	1.58
Mg#	61	61	45	78	66	68	71	60	63	68	76	61	55	56

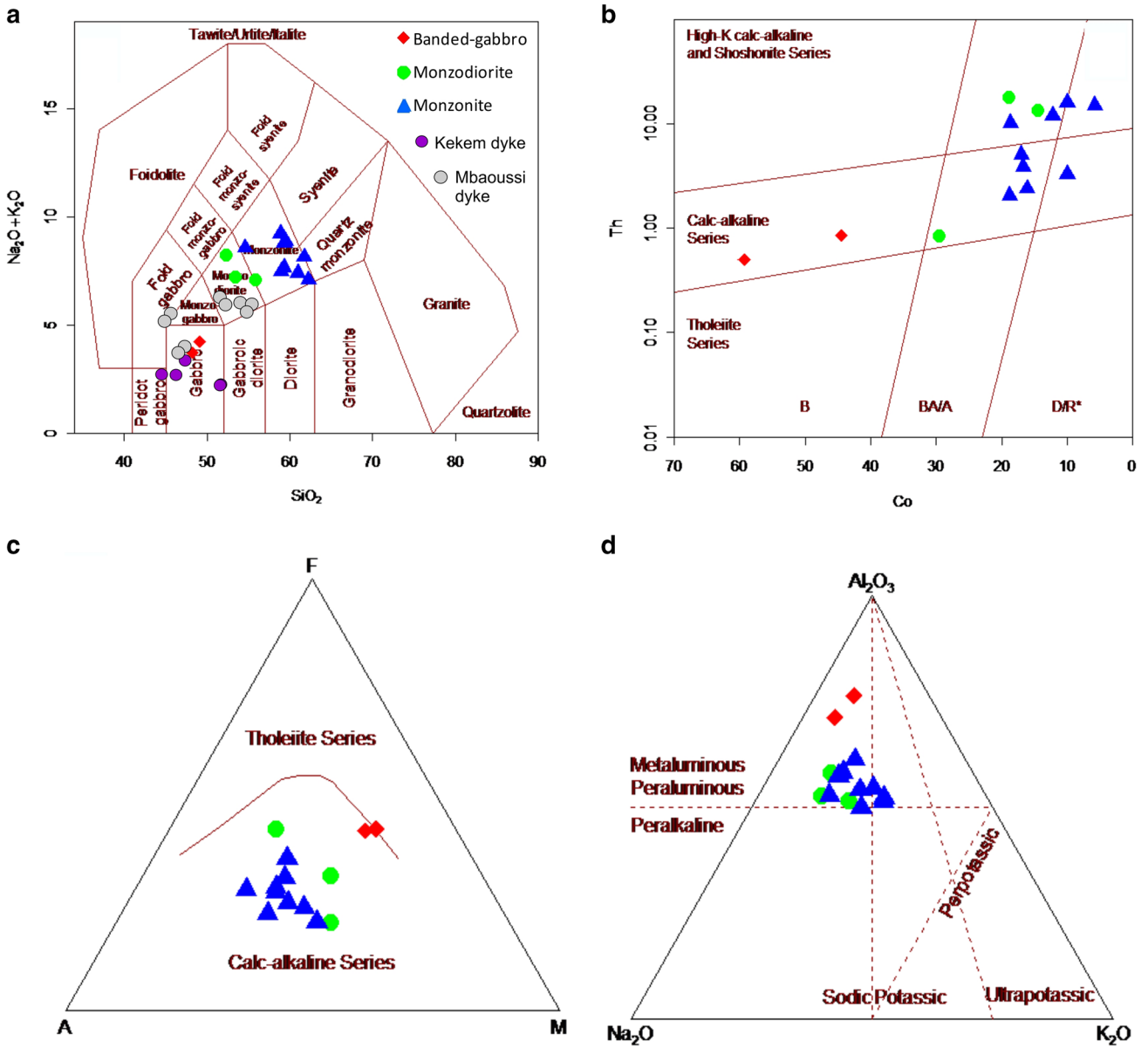

Fig. 6 **a** Total alkali silicate (TAS) classification diagram for the studied dykes according to [30], **b** Co–Th diagram [31], **c** AFM diagram by [32], **d** Na_2O–K_2O–Al_2O_3 diagram

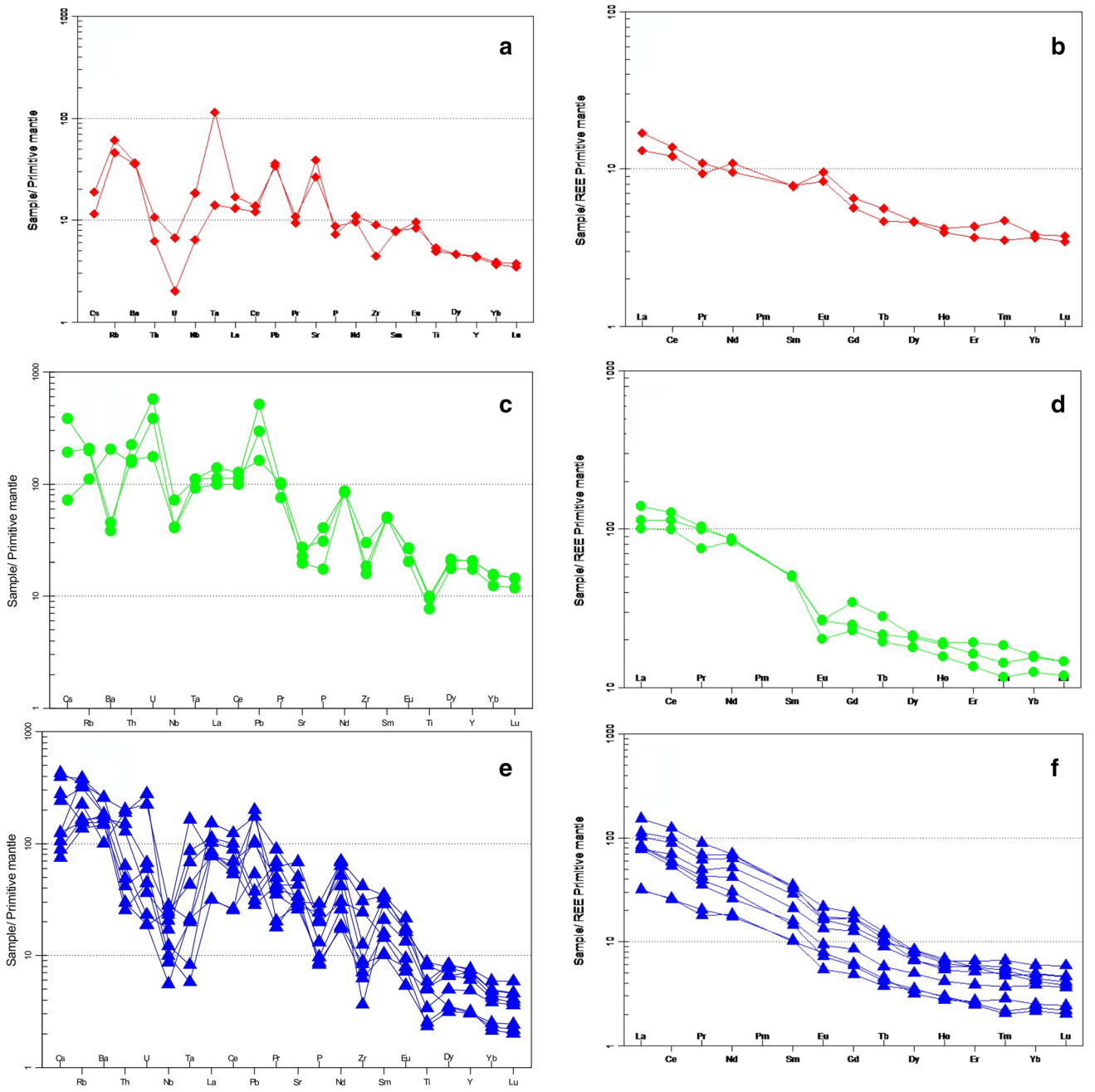

Fig. 7 Normalized multi-element and primitive REEs diagrams: **a**, **b** for the banded gabbros, **c**, **d** for the monzodiorite and **e**, **f** for the monzonites

also been demonstrated that samples contaminated by the earth's crust generally show a significant enrichment in LREE with flat HREE patterns [37–41].

Taking into account these geochemical criteria, it can be suggested that the mafic dykes studied samples (banded gabbro) are not contaminated or, if they are contaminated, the rate would be negligible since they present almost flat REE profiles, and no significant Nb and Zr anomaly, but only a positive Sr anomaly on multiple element patterns (Fig. 7a, b). Moreover, banded gabbro samples show low Ba contents (235–242 ppm) compared to the mid-continental crust (Ba = 259–628 ppm; [42]). In addition, they exhibit low Lu/Yb ratios (0.14–0.15) similar to those of mantle-derived magmas (0.14–0.15) but lower than those of continental crustal magmas (0.16–0.18) [42], thus excluding the idea of significant crustal contamination of the magma of banded gabbro during their evolution.

According to [42, 43], negative anomalies of Nb, Ta and Ti are typical of continental crust and rocks whose chemical composition has been modified by subduction [44]. Depletion in Nb, Ta or Ti of the intermediate dykes would indicate a contribution of the crust to their formation [37–41].

The intermediate dyke samples show inclined REE profiles, negative Nb and Ta anomalies and a variable Sr anomaly [negative Sr anomaly for the monzodiorite (Fig. 7c, d); positive Sr anomaly for the monzonites on the multiple elements profiles (Fig. 7e, f)] thus indicating a possibility of crustal contamination.

5.2 Petrogenesis and magma source

Several studies have shown that that high field strength elements (HFSE) such as Zr, Hf, Nb, Ta, Th, Y, P and Ti are immobile even after high degree metamorphism [45–48]. However, large ion lithophile elements (LILE) like Ba, Cs, and Rb have extreme fractionation between the earth's crust and mantle, and can be mobile during metamorphism or crustal contamination during rise of the magma, thus modifying the physical/chemical composition of the magma [49, 50]. Thus, HFSE and transition metals (Sc, V, Cr and Ni) are most often used to study the petrogenesis of rocks including the sources of magma and the tectonic contexts of rocks because of their relative stability during metamorphism or crustal contamination [51–55]. The geochemistry of the major elements of the studied banded gabbro demonstrates the calc-alkaline nature of their parental magma, even though a sample of banded gabbro falls on the boundary between the tholeiite and calc-alkaline series of the AFM diagram of [32] (Fig. 6c). The chemical composition of banded gabbros (Sect. 4.3.1) compared to that of monzodiorites and monzonites (Sects. 4.3.2. and 4.3.3) indicates different sources or different processes governing the formation of mafic dykes (banded gabbros) and intermediate dykes (monzonites and monzodiorites).

These values also show that the banded gabbros probably resulted from much evolved mantle parental magma [56] and a certain degree of minerals fractionation (such as olivine and clinopyroxene which are rich in Cr and Ni).

It is widely known that intermediate magma can be formed by several processes, including the AFC (assimilation and fractional crystallization) process of mantle-derived magma, partial melting of the metasomatized mantle wedge, and partial melting of crustal material [57–59], or may come from the interaction of coeval mafic and felsic magmas [60]. The absence of mafic enclaves or mafic-felsic mingling in the study area excludes the last hypothesis.

The intermediate dikes may have been generated by the partial fusion of the garnet-lherzolite mantle enriched in highly incompatible trace elements, and depleted in Nb and Ta by a metasomatism of the fluids derived from the subduction.

Cullers and Graf [61–63] have shown that the gradient of REE patterns of any sequence of rocks is useful for understanding melting conditions. It is suggested that a low percentage of mantle source fusion can produce slightly fractionated (inclined) REE patterns, while flat REE patterns are produced by a higher degree of mantle fusion [63]. An inclined REE pattern indicates origin from an enriched mantle source, while flat REE patterns demonstrate a depleted mantle source. The REE profiles of the banded gabbro samples are relatively flat (Fig. 7b), suggesting a high degree of partial melting from a depleted mantle source. The REE patterns of the monzodiorite and monzonite samples are inclined (Fig. 7d, f) and ultimately indicate their derivation from a relatively low degree of partial melting from an enriched mantle source. The samples of the intermediate dykes (Monzodiorites and monzonites) show enriched LREE and almost flat HREE profiles indicating some involvement of the crust in their genesis.

The weak negative Eu anomalies ($Eu/Eu^* = 0.60–0.99$) for the intermediate dykes attest to a probable fractionation of the plagioclase [47] or could show that the plagioclase was retained at the source in the case of partial fusion of the mantle source [64].

The banded gabbros show slightly negative anomalies in P and Ti (Fig. 7a) thus justifying the limited role of Fe–Ti oxides and the fractionation of apatite [65] unlike monzodiorite and monzonite (Fig. 7c, e) which have well-marked negative anomalies in P and Ti, indicating the presence of Fe–Ti oxides and the fractionation of the apatite.

In addition, the analyzed intermediate dyke samples show obvious negative anomalies in Zr, Ti and P, and positive anomalies in Rb and Ba (Fig. 7c, e). The enrichment in Rb and Ba of the intermediate dykes would probably come from the mobilization caused by the subducted crust. Considering the fact that the study area is a shear zone, the contribution of metamorphism during shear events should not be totally excluded.

The LaN/SmN and DyN/YbN ratios are very useful in understanding the degree of fusion and the composition of the source [62, 66]. Thus, on the LaN/SmN versus DyN/YbN diagram normalized to the chondrite of [62] (Fig. 8a), the samples of the mafic dykes (banded gabbro) lie near the fusion curve 2.7–2, 8 Gpa and have a DyN/YbN ratio < 1.3. On the other hand, the intermediate dyke samples (monzodiorite and monzonite) lie between the fusion curves at 2.7 and 3 Gpa and have a high DyN/YbN ratio; the monzodiorite samples in particular lies between the melting curve 2.9–3 Gpa. Two monzonite samples are not included in this plot because they have a higher LaN/SmN ratio (~ 4). According to [67], the lower pressure limit for

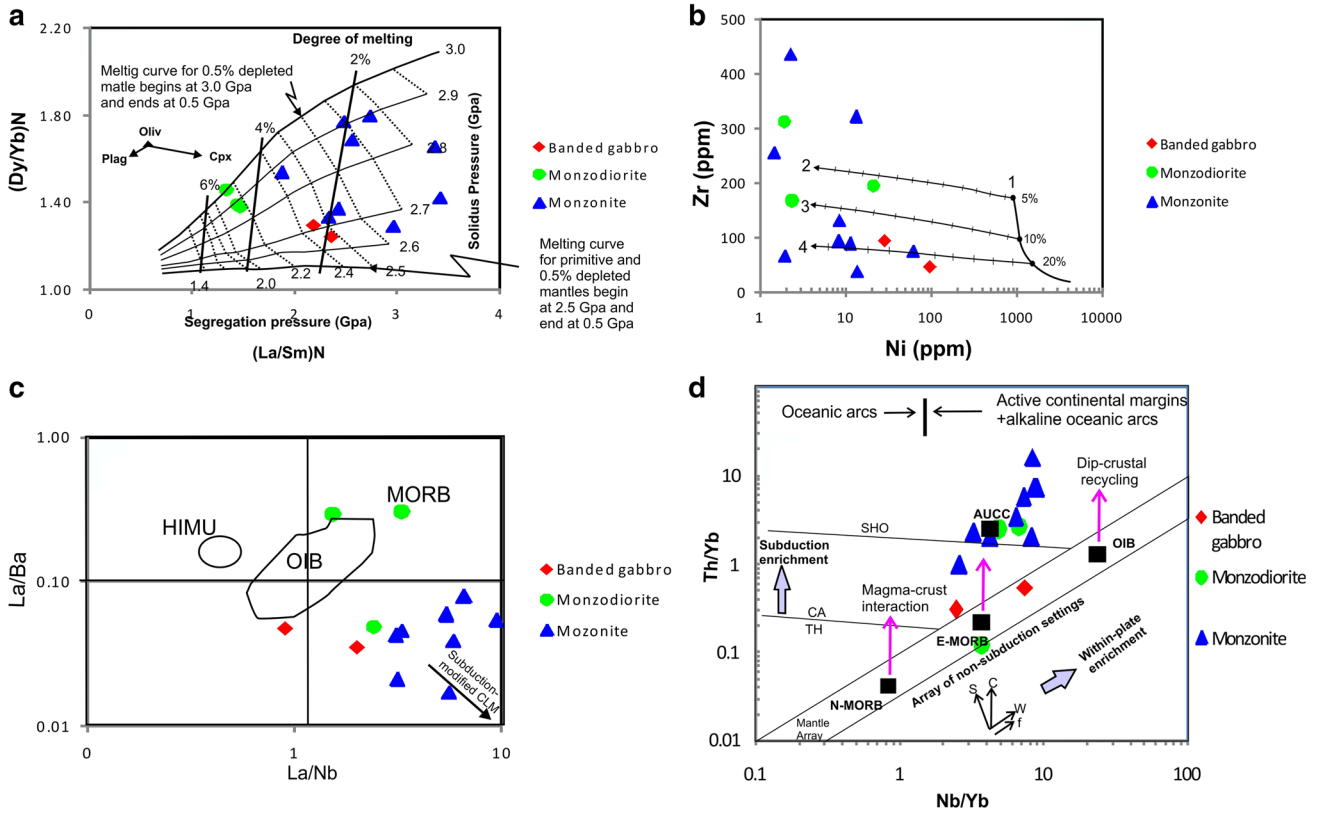

Fig. 8 **a** Chondrite-normalized LaN/SmN and DyN/YbN ratios for mantle melting models using the algorithm of [62] for primitive mantle depleted by 0.5% melting (after [66]. Other parameters are as specified by [66]. Chondrite values are taken from [29]. Model curves, for melting starting at 3.0, 2.9, 2.8, 2.7, 2.6 and 2.5 GPa and ending at 0.5 GPa, define a melting grid, where solid sub-vertical lines contour constant mean melt fraction, whereas the dashed sub-vertical lines contour final pooled melt segregation pressure (after [66]). **b** Trace elements modeling based on Ni versus Zr. (after [68]) considering melting of a Iherzolite mantle source (composition: 11 ppm Zr and 2000 ppm Ni; as given by [69] at the depths of 80–100 km. Curve 1 denotes batch melting at 1500 °C (1 atm equivalent) with degrees of melting noted in percentage. Curves 2, 3 and 4 represent olivine fractionation with percentage of olivine removal noted in 5% increments. **c** La/Ba versus La/Nb diagram (after [70]). **d** Th/Yb versus Nb/Yb for the studied mafic and intermediate dykes. The mantle arrey includes constructive magma plate boundaries (*NMORB* Normal Mid-Ocean Ridges Basalts, *E-MORB* Enriched Mid-Ocean Ridge Basalts) and within-plate alkaline basalts (*OIB* Ocean Island Basalts). AUCC is Archean Upper Continental Crust. Fields for convergent margin basalts include the tholeiitic (TH), calc-alkaline (CA) and shoshonitic (SHO) magma series. The vectors S, C, W and f refer to subduction zone component, crustal contamination, within plate fractionation and fractional crystallization, respectively [71]

the mantle stability of garnet is between 2.5 and 2.8 GPa, while garnet and spinel can coexist up to ~ 3.0 GPa. Thus, it can be suggested that banded gabbros are probably generated in the garnet stability field, while monzodiorites may be derived from magma generated in the spinel stability field. As for monzonites, they may be formed from melt generated within both garnet and spinel fields.

In the Ni–Zr petrogenetic diagram after [68, 69, 72], used to model the processes of fusion or differentiation of the Earth's mantle (Fig. 8b), the banded gabbro samples fall around and slightly above the olivine fractionation curve 4, demonstrating their derivation from a melt generated by 15–20% melting of a mantle source. The monzodiorite samples probably originate from a slightly lower melting percentage (< 10%) from the mantle source. On the other hand, the monzonite samples suggest a varying degree of melting. A number of experimental works [63, 73, 74] suggest that subalkaline tholeiitic magma can be generated by the fusion of 15 to 30% of the upper mantle peridotite, while any fusion of less than 10% of the peridotite of the mantle can produce an alkaline-rich basalt melt.

Therefore, the banded gabbro samples are likely derived from subalkaline tholeiitic magma, while monzodiorites are from alkaline rich basaltic melt. The inclined REE patterns of monzodiorites also support a lower percentage of mantle source fusion.

Rock formed from AFC process during magma rise generally has high Nb/La and La/Sm ratios (Nb/La > 0.5, La/Sm > 5.0; [75]) which are closed to the ratios of the crust. The intermediated dykes show Nb/La varying from 0.11 to

0.65 and La/Sm from 3.1 to 9.0 demonstrating the input of crustal component or the sub-continental lithospheric mantle (SCLM) modified by subducted slab-derived fluids [76] in the generation of the intermediate dykes.

Moreover, giving the fact that Th/La ratio is a useful proxy in identifying subduction-related magmas [77], the mafic and intermediate dykes of the Tikar plain show low Th/La ratios (0.06–0.29) indicating subduction-related magmas.

The intermediate dykes show high Th/Nb (0.23–1.90) ratios and relatively negative Nb–Ta anomalies for the majority of the samples on the primitive mantle-normalized trace element patterns (Fig. 7c, e), consistent with derivation from subducted lithospheric slab with significant crustal materials. The variations on HFSE and LILE values of the intermediate dykes (monzodiorite and monzonites) are probably due to the influx of fluids associated with subduction [50].

The Mafic dykes (banded gabbro) have a markedly low (La/Yb) N ratio (3.48–4.74; Table 1; Fig. 7), which shows a significantly higher degree of partial melting in the source. The intermediate dykes have significantly negative Zr negative and Nb–Ta anomalies (Fig. 7c, e), which are characteristics of metasomatism in the source zone. The dikes show a metasomatized sub-continental lithospheric mantle (SCLM) trend on the La/Nb versus La/Ba diagram (Fig. 8c), after [70], and lithospheric mantle metasomatism may be related to fluid or sediment input [78].

On the Nb/Yb versus Th/Yb diagram (Fig. 8d), the mafic dyke samples fall around the E-MORB, while the intermediate dyke samples plot very close to the domain to the average continental crust (ACC) suggesting the role of the crust in their genesis. This may suggest that the mantle source was modified (metasomatized) by the crustal component, probably during the subduction event.

On the Sm/Yb versus La/Sm diagram, the dyke dataset falls well above the spinel facies and closer to the garnet facies trend involving low degree of partial melting in the garnet-peridotite facies (probably between 80 and 100 km deep). This claim is supported by the overlap of the REE patterns of mafic dykes and intermediate dykes indicating two types of source or the process during the evolution of the magmas. The scattering of the samples along the contamination vector on the Th/Yb versus Nb/Yb diagram (Fig. 9) could show the possible implication of the subducted lithosphere with crustal component addition.

5.3 Tectonic setting

On the discrimination diagram of Ti/100–Zr–Sr/2 [51], the dykes plot in the island arc tholeiite domain (IAT) (Fig. 10a). The studied dykes have petrographic (presence of sheared or delta-shaped and sigma-shaped porphyroblasts, fish-shaped amphibole, presence of folds and foliation, cataclastic and mylonitic textures) and geochemical features attesting to their emplacement in a compressive and transcurrent tectonics context [20]. The magma generated by the subducted lithosphere may have followed the shear axes and sub-vertical faults to settle in the granito-gneissic crust [20].

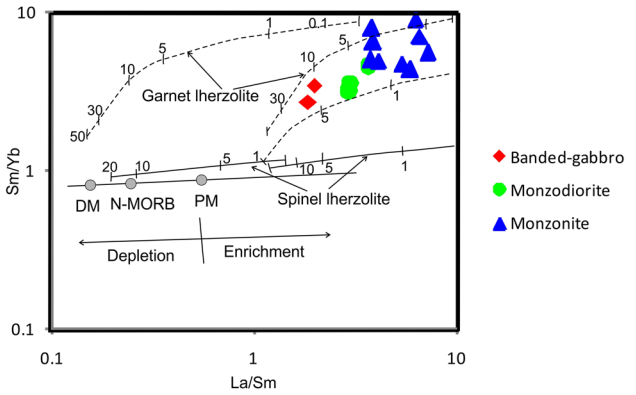

Fig. 9 Sm/Yb versus La/Sm for the studied dykes. Mantle arrey (thick line) is defined by depleted MORB mantle (DMM) [79] and the primitive mantle (PM) [49]; the melting curves for lherzolite spinel and peridotite garnet with the compositions DMM and PM are according to [80]. The numbers along the lines represent the degree of partial melting

It has been established that the intermediate rocks (monzonites and monzodiorite) can be derived through anatexis of mafic rocks from the lower crust or via partial melting of enriched mantle material [82, 83]. The high Mg# (≈64) of the intermediate dykes of the Tikar plain preclude an origin via anatexis of mafic rocks from the lower crust, as the Mg# content in melt from the lower crustal source is usually less than 60. According to [83–85], partial melting of the delaminated lower crust in an intra-continental setting with contribution from peridotite can result in the formation of intermediate rocks.

The monzonites and monzodiorites plot in the Volcanic Arc Granites (VAG) and Within Plate Granites (WPG) fields (Fig. 10b), respectively. They are similar to the Batouri granitoids in East Cameroon [86] and Gwangcheon area, Hongseong Belt, in South Korea [87].

The high-K, calc-alkaline affinities of intermediate dykes are consistent with granitoids formed in active continental margins [81]. All These characteristics conform to the geodynamic model of subduction involving sub-crustal lithospheric delamination, and/ or and break-off of the lithospheric slab beneath the Adamawa Yade domain [11]. This model demonstrates that the collision between the mobile belt and the northern edge of the Congo craton would have caused the crustal thickening, sub-crustal lithospheric delamination and upwelling

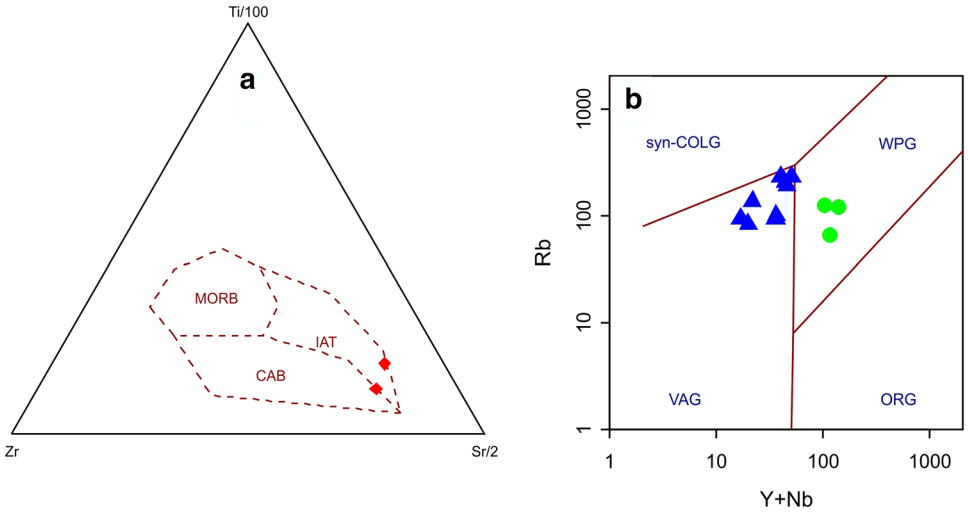

Fig. 10 **a** Discrimination diagram of Ti/100–Zr–Sr/2 [51] the mafic dyke samples plot in the island arc tholeiite (IAT) area, **b** geotectonic diagram [81] for intermediate dykes

of the asthenosphere. These processes would have generated excess heat that melted the crustal rocks at depth and produced high-K calc-alkaline magmas [11]. Therefore, it may be also possible that changes in the Th/Nb, Th/Ta, La/Nb and Ce/Pb ratios observed on some intermediate dykes may be due to the injection of asthenospheric magmas from beneath the slab break-off to the mantle wedge [83–85].

Strike-slip faults may have facilitated the injection of mafic magmas into the base of the lower crust. Partial melting at the base of the lower crust and/or mantle wedge most likely formed the intermediate dyke magmas. Then, during later sinistral and dextral shearing, the mafic and intermediate magmas were channeled into the shears and sub-vertical fault axes toward the crust [20, 88]

5.4 Comparison with other dykes from the Central African Fold Belt in Cameroon

The differences between the dykes of the Tikary plain (in the central part of the central Cameroon shear zone (CCSZ)), the dolerite dykes of Mbaoussi (in the Adamawa plateau [89]) and the dykes of Kekem (in the southwestern part of CCSZ [90]) are highlighted in Fig. 11a, b. The dykes of the Tikar Plain are different from those of the Kekem zone, which have higher HREE contents even though they show negative Nb anomalies in the multi-element diagram like those of the Tikar Plain (Fig. 11a). The Mbaoussi dykes appear to be more similar to the Tikar plain dykes, showing enrichment in LREE and depletion in HREE (Fig. 11a).

The dykes of the Tikar plain, the Kekem dykes and the Mbaoussi dyke may derive from the same of the

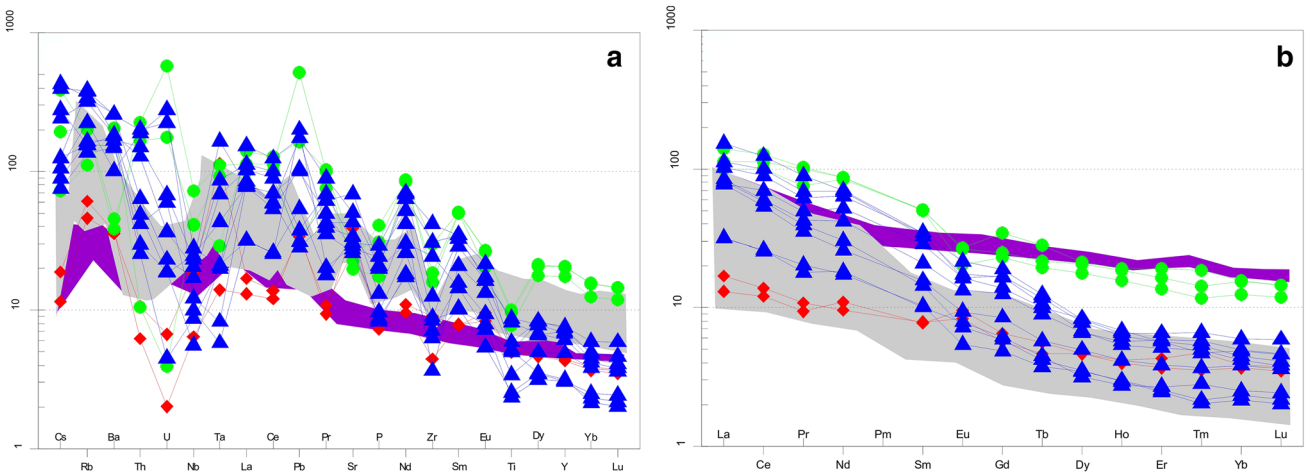

Fig. 11 **a** Primitive mantle-normalized incompatible trace elements for the Tikar plain dykes compared to Kekem and Mbaoussi dykes; **b** chondrite-normalized REE for the Tikar plain dykes compared to Kekem and Mbaoussi dykes. The data for the Kekem dykes are from [90] and the Mbaoussi dykes' data are from [89]. The normalization values are from [29]

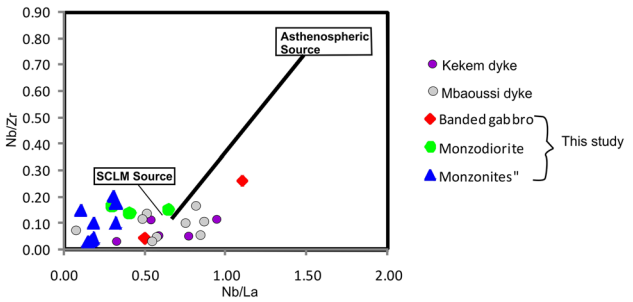

Fig. 12 Nb/La versus Nb/Zr discrimination diagram after [96] showing the sub-continental lithospheric mantle source (SCLM) for The Tikar plain, Kekem, and Mbaoussi dykes

subcontinent lithospheric mantle source (Fig. 12). In general, magmas with high Mg and Ni contents suggest a magmatism related to the activity of the plume [91] and a tholeiitic affinity indicates a lithospheric extension [9, 91–93]. Therefore, the role played by a plume-lithosphere interaction should not be excluded as suggested by [91]. From a regional point of view, the Mbaoussi area, the Tikar plain and the Kekem area belong to the Adamawa domain of the Pan-African Fold Belt in Cameroon, suggesting that these dyke swarms could belong to a same magmatic episode. Consequently, the late dextral shear movement [dated at 552 Ma (EMP dating on monazite [94])], along the Central Cameroon Shear Zone, may have served as a path for the dyke's magma during their ascent towards the surface. This idea is consistent with the layout of the pan-African fracture network and the hypothesis of a reactivation or re-play of the Pan-African structures associated with the dyke swarms of the Pan-African North Equatorial Fold Belt [95]. The geochronological data that may clarify the emplacement ages of these dykes are not yet been established.

6 Conclusion

Based on field relationships, petrographic evidences and geochemical compositions, the Tikar plain dykes are classified as banded-gabbro for the mafic dykes and monzodiorites and monzonites for the intermediate dykes. They have a porphyritic to porphyroblastic and cataclastic to mylonitic textures with deformation features such as shears, sigma "σ" and delta "θ" porphyroblasts, and "amphibole fish" porphyroblasts testifying to their syn-tectonic emplacement.

The dykes are high-K calc-alkaline to shoshonitic in nature. They are enriched in LREE and depleted in HREE. The geochemistry of their rare-earth elements and trace elements indicates that the intermediate dykes of the Tikar plain might have been generated from subducted lithospheric slab with addition of significant crustal component.

The mafic dykes plot in island arc tholeiite (IAT) and in calc-alkaline basalts (CAB) domains, while the intermediate ones plot in the Volcanic Arc VAG and Within Plate Granite (WPG) domains. The geochemical characteristics of the mafic to intermediate dykes suggest their derivation from a various degree of partial melting in the garnet spinel facies probably between depths of 80 and 100 km. They are geochemically similar to other dykes from the Adamawa Yade domain of the Central African Fold Belt in Cameroon. The collision between the Central African Fold Belt and the northern edge of the Congo Craton resulting in crustal thickening, sub-crustal lithospheric delamination, and upwelling of the asthenosphere may have been the principal process in the generation of the intermediate dykes from the Tikar plain. The dykes may have used the shear C_3 and the sub-vertical faults as conduits for intrusion during the last deformation phase D_3.

Compliance with ethical standards

Conflict of interest On behalf of all authors, the corresponding author states that there is no conflict of interest.

References

1. Tchameni R, Pouclet A, Mezger K, Nsifa NE, Vicat JP (2004) Single zircon Pb–Pb and Sm–Nd whole-rock ages for the Ebolowa greenstone belts: evidence for pre-2.9 Ga terranes in the Ntem complex (South Cameroon). J Cameroon Acad Sci 4:235–246
2. Shang CK, Satir M, Nsifa EN, Liegeois JP, Siebel W, Taubald H (2007) Archaean high-K granitoids produced by remelting of earlier tonalite–trondhjemite–Granodiorite (TTG) in the Sangmelima region of the Ntem Complex of the Congo craton, southern Cameroon. Int J Earth Sci 96:817–841
3. Li XH, Chen Y, Li J, Yang C, Ling XX, Tchouankoue JP (2016) New isotopic constraints on age and origin of Mesoarchean charnockite, trondhjemite and amphibolite in the Ntem Complex of NW Congo Craton, southern Cameroon. Precambrian Res 276:14–23

4. Nzenti JP, Barbey P, Tchoua FM (1999) Evolution crustale au Cameroun: elements pour un modele geodynamique de l'orogenese neoproterozoique. In: Vicat JP Bilong P (eds) Geologie et environnements au Cameroun. Collection GEOCAM. pp 397–407
5. Nzenti JP, Minyem D, Tchouankoue JP, Belinga SE (2001) Le Panafricain. In: Belinga SE (ed) Histoire Geologique du Cameroun. Les Classiques Camerounais. pp 39–55
6. Toteu SF, Van Schmus WR, Penaye J, Michard A (2001) New U-Pb and Sm–Nd data from North-central Cameroon and its bearing on the prePan African history of central Africa. Precambrian Res 108:45–73
7. Njiekak G, Dorr W, Tchouankoue JP, Zulauf G (2008) U-Pb zircon and microfabric data of (meta) granitoids of western Cameroon: constraints on the timing of pluton emplacement and deformation in the Pan-African belt of Central Africa. Lithos 102:460–477
8. Bouyo Houketchang M, Penaye J, Barbey P, Toteu SF, Wandji P (2013) Petrology of high pressure granulite facies metapelites and metabasites from Tchollire´ and Banyo regions: geodynamic implication for the Central African fold belt (CAFB) of North-central Cameroon. Precambrian Res 224:412–413
9. Maluski H, Coulon C, Popoff M, Baudin P (1995) 40Ar/39Ar chronology, petrology and geodynamic setting of Mesozoic to early Cenozoic magmatism from the Benue Trough, Nigeria. J Geol Soc Lond 152:311–326
10. Toteu SF, Van Schmus WR, Penaye J, Michard A (2001) New U–Pb and Sm–Nd data from north-central Cameroon and the pre-Pan-African history of central Africa. Precambr Res 108:45–73
11. Toteu SF, Penaye J, Djomani YP (2004) Geodynamic evolution of the Pan-African belt in central Africa with special reference to Cameroon. Can J Earth Sci 41:73–85
12. Penaye J, Kröner A, Toteu SF, Van Schmus WR, Doumnang J-C (2006) Evolution of the Mayo Kebbi region as revealed by zircon dating: an early (ca. 740 Ma) Pan-African magmatic arc in southwestern Chad. J Afr Earth Sci 44:530–542
13. Nzenti JP, Barbey P, Macaudiere J, Soba D (1988) Origin and evolution of late Precambrian high-grade Yaounde gneisses (Cameroon). Precambrian Res 38:91–109
14. Toteu SF, Macaudière J, Bertrand JM, Dautel D (1990) Metamorphic zircons from North Cameroon: implications for the Pan-African evolution of Central Africa. Geol Rundsch 79:777–788
15. Toteu SF, Yongué Fouateu R, Penaye J, Tchakounté J, Semé Mouangué AC, Van Schmus WR, Deloule E, Stendal H (2006) U-Pb dating of plutonic rocks involved in the nappe tectonic in southern Cameroon: consequence for the Pan-African fold belt. J Afr Earth Sci 44:479–493
16. Nkoumbou C, Yonta Ngouné C, Villiéras F, Njopwouo D, Yvon J, Ekodeck GE, Tchoua FM (2006) Découverte de roches à affinité ophiolitiques dans la chaîne panafricaine au Cameroun: les talcschistes de Ngoung, Lamal Pougué et Bibodi Lamal. C R Géosci 338:1167–2117
17. Penaye J, Toteu SF, Michard A, Bertrand JM, Dautel D (1989) Reliques granulitiques d'âge protérozoïque inférieur dans la zone mobile panafricaine d'Afrique centrale au Cameroun; géochronologie U-Pb sur zircons. C R Acad Sci Paris 309:315–318
18. Ganwa AA (2005) Les granitoïdes de Meiganga: etude petrographique, geochimique, structurale et geochronologique. Leur place dans la chaîne pan-africaine (These de doctorat d'Etat). Univ. Yde I. p 162
19. Tchameni R, Pouclet A, Penaye J, Ganwa AA, Toteu SF (2006) Petrography and geochemistry of the Ngaoundere Pan-African granitoids in Central North Cameroon: implications for their sources and geological setting. J Afr Earth Sci 44:543–560
20. Ntiéche B, Mohan MR, Moundi A (2017) Granitoids of the Magba Shear Zone, West Cameroon, Central Africa: evidences for emplacement under transpressive tectonic regime. J Geol Soc India 89:33–46
21. Njonfang E, Ngako V, Kwékam M, Affaton P (2006) Les orthogneiss calco-alcalins de Foumban–Bankim: témoins d'une zone de cisaillement de haute température. C R Geosci 338:606–616
22. Dumont JF (1986) Identification par teledetection de l'accident de la Sanaga (Cameroun). Sa position dans le contexte des grands accidents d'Afrique Centrale et de la limite nord du craton congolais. Geodynamique 1:13–19
23. Ngako V, Affaton P, Nnange JM, Njanko T (2003) Pan-African tectonic evolution in central and southern Cameroon; transpression and transtension during sinistral shear movements. J Afr Earth Sci 36:207–214
24. Njanko T, Nedelec A, Affaton P (2006) Synkinematic high-K calc-alkaline plutons associated with the Pan-African Central Cameroon Shear Zone (W Tibati area): petrology and geodynamic significance. J Afr Earth Sci 44:494–510
25. Ganwa AA, Siebel W, Frisch W, Shang Kongnyuy C (2011) Geochemistry of magmatic rocks and time constraints on deformational phases and shear zone slip in the Meiganga area, central Cameroon. Int Geol Rev 33(7):759–784
26. Dumort J-C (1968) Carte géologique de reconnaissance à l'échelle du 1/50000ième, République Fédérale du Cameroun, Notice explicative sur la feuille Douala Ouest, Direction des Mines et de la Géologie du Cameroun
27. Ntiéche B, Mohan MR, Moundi A, Mounjouohou MA (2016) Petrogenesis and Geochemical Characterization of the Granitoids of the Magba Shear Zone West Cameroon Central Africa. Open J Geol 6:812–839
28. Krishna AK, Murthy NN, Govil PK (2007) Multi element analysis of soils by wavelength dispersive X-ray fluorescence spectrometry. At Spectrosc 28:202–214
29. McDonough WF, Sun SS (1995) The composition of the earth. Chem Geol 120:223–253
30. Middlemost EAK (1985) Magmas and magmatic rocks. Longman, London
31. Hastie AR, Kerr AC, Pearce JA, Mitchell SF (2007) Classification of altered volcanic island rocks using immobile trace elements: development of the Th–Co discrimination diagram. J Petrol 48:2341–2357
32. Irvine TN, Baragar WRA (1971) A guide to the chemical classification of the common volcanic rocks. Canad J Earth Sci 8:523–548
33. Lechler PJ, Desilets MO (1987) A review of the use of loss on ignition as a measurement of total volatiles in whole-rock analysis. Chem Geol 63:341–344
34. Gill RCO, Bridgwater D (1979) Early Archaean basic magmatism in west Greenland: the geochemistry of the Ameralik dykes. J Petrol 20:695–726
35. Kalsbeek F, Taylor PN (1986) Age and origin of early proterozoic dolerite dykes in southwest Greenland. Contrib Miner Petrol 89:307–316
36. Tarney J, Weaver BL (1987) Geochemistry and petrogenesis of early Proterozoic dyke swarms. In: Halls HC, Fahrig WF (eds) Mafic Dyke Swarms. Geological Association of Canada Special Paper 34. pp 81–94
37. Crawford AJ (1989) Boninites and related rocks. Unwin Hyman, London
38. Tatsumi Y, Eggins SM (1995) Subduction zone magmatism. Blackwell, Oxford
39. Srivastava RK, Singh RK (2004) Trace element geochemistry and genesis of the Precambrian sub-alkaline mafic dykes from central India craton: evidence for mantle metasomatism. J Asian Earth Sci 23:373–389
40. Zhao JH, Zhou MF (2007) Geochemistry of neoproterozoic mafic intrusions in the Panzhihua district (Sichuan Province, SW China): implications for subduction-related metasomatism in the upper mantle. Precambr Res 152:27–47

41. Cai K, Sun M, Yuan C, Zhao G, Xiao W, Long X, Wu F (2010) Geochronological and geochemical study of mafic dykes from the northwest Chinese Altai: implications for petrogenesis and tectonic evolution. Gondwana Res 18:638–652
42. Rudnick RL, Gao S (2003) Composition of the continental crust. Treatise Geochem 3:1–64
43. Frey FA, Weis D, Borisova A, Yu XuG (2002) Involvement of continental crust in the formation of the Cretaceous Kerguelen Plateau: new perspectives from ODP Leg 120 sites. J Petrol 43:1207–1239
44. Ernst RE, Bleeker W, Söderlund U, Kerr AC (2013) Large igneous provinces and supercontinents: toward completing the plate tectonic revolution. Lithos 174:1–14
45. Pearce JA (1975) Basalt geochemistry used to investigate past tectonic environments on Cyprus. Tectonophysics 25:41–67
46. Manikyamba C, Kerrich R, Khanna TC, Satyanarayanan M, Krishna AK (2009) Enriched and depleted arc basalts, with Mg-andesites and adakites: a potential paired arc-back-arc of the 2.6 Ga Hutti greenstone terrane, India. Geochim Cosmochim Acta 73:1711–1736
47. Wang YJ, Zhang AM, Cawood PA, Fan WM, Xu J, Zhang G, Zhang Y (2013) Geochronological, geochemical and Nd–Hf–Os isotopic fingerprinting of an early neoproterozoic arc-back-arc system in South China and its accretionary assembly along the margin of Rodinia. Precambr Res 231:343–371
48. Santosh M, Hu CN, He XF, Li SS, Tsunogae T, Shaji E, Indu G (2017) Neoproterozoic arc magmatism in the southern Madurai block, India: subduction, relamination, continental outbuilding, and the growth of Gondwana. Gondwana Res 45:1–42
49. Sun SS, McDonough WF (1989) Chemical and isotopic systematics of oceanic basalts: implications for mantle composition and processes. In: Saunders AD, Norry MJ (eds) Magmatism in the Ocean Basins, vol 42. Geological Society of Special Publication, London, pp 313–345
50. Staudigel H, Plank T, White B, Schmincke HU (1996) Geochemical fluxes during seafloor alteration of the basaltic upper oceanic crust: DSDP sites 417 and 418. In: Bebout GE, Scholl SW, Kirby SH, Platt JP (eds) Subduction top to bottom. American Geophysical Union, Washington, DC, pp 19–38
51. Pearce JA, Cann JR (1973) Tectonic setting of basic volcanic rocks determined using trace element analyses. Earth Planet Sci Lett 19:290–300
52. Winchester JA, Floyd PA (1976) Geochemical magma type discrimination; application to altered and metamorphosed basic igneous rock. Earth Planet Sci Lett 28:459–469
53. Floyd PA, Winchester JA (1978) Identification and discrimination of altered and metamorphosed volcanic rocks using immobile elements. Chem Geol 21:291–306
54. Rollinson HR (1993) Using geochemical data: evaluation, presentation, interpretation. Longman, Essex
55. Jochum KP, Verma SP (1996) Extreme enrichment of Sb, Tl, and other trace elements in altered MORB. Chem Geol 130:289–299
56. Ahijado A, Casillas R, Hernandez-Pacheco A (2001) The dyke swarms of the Amanay Massif, Fuerteventura, Canary Islands (Spain). J Asian Earth Sci 19:333–345
57. Wang JP, Li XW, Ning WB (2019) Geology of a neoarchean suture: evidence from the Zunhua Ophiolitic Mélange of the Eastern Hebei Province North China Craton. GSA Bull. https://doi.org/10.1130/b35138.1
58. Thompson AB (1996) Fertility of Crustal Rocks during Anatexis. Earth Environ Sci Trans R Soc Edinb 87(1/2):1–10. https://doi.org/10.1017/s0263593300006428
59. Arnaud NO, Vidal P, Tapponnier P (1992) The high K_2O volcanism of northwestern tibet: geochemistry and tectonic implications. Earth Planet Sci Lett 111(2):351–367. https://doi.org/10.1016/0012-821x(92)90189-3
60. Barbarin B (2005) Mafic magmatic enclaves and mafic rocks associated with some granitoids of the central Sierra Nevada batholith, California: nature, origin, and relations with the hosts. Lithos 80:155–177
61. Cullers RL, Graf JL (1984) Rare earth elements in igneous rocks of the continental crust: predominantly basic and ultrabasic rocks. In: Henderson P (ed) Rare earth element geochemistry. Elsevier, Amsterdam, pp 237–274
62. Fram MS, Lesher CE (1993) Geochemical constraints on mantle melting during creation of the North Atlantic basin. Nature 363:712–715
63. Hirschmann MM, Ghiorso MS, Wasylenki LE, Asimow PD, Stolper EM (1998) Calculation of peridotite partial melting from thermodynamic models of minerals and melts. I. Method and composition to experiments. J Petrol 39:1091–1115
64. Frost BR, Barnes CG, Collins WJ, Arculus RJ, Ellis DJ, Frost CD (2001) A geochemical classification for granitic rocks. J Petrol 42:2033–2048
65. Zhang YZ, Wang YJ, Fan WM, Zhang AM, Ma LY (2012) Geochronological and geochemical constraints on the metasomatised source for the Neoproterozoic (~825 Ma) high-mg volcanic rocks from the Cangshuipu area (Hunan Province) along the Jiangnan domain and their tectonic implications. Precambr Res 220–221:139–157
66. Mayborn KR, Lesher CE (2004) Paleoproterozoic mafic dyke swarms of northeast Laurentia: products of plumes or ambient mantle? Earth Planet Sci Lett 225:305–317
67. Robinson JAC, Wood BJ (1998) The depth of the spinel to garnet transition at the peridotite solidus. Earth Planet Sci Lett 164:277–284
68. Condie KC, Bobrow DJ, Card KD (1987) Geochemistry of Precambrian mafic dykes from the Southern Superior Province. In: Halls HC, Fahrig WF (eds) Mafic Dyke Swarms, vol 34. Geological Association of Canada Special Paper. pp 95–108
69. Rajamani V, Shivakumar K, Hanson GN, Shirey SB (1985) Geochemistry and petrogenesis of amphibolite, Kolar Schist belt, South India; evidence for komatiitic magma derived by low percentage of melting of the mantle. J Petrol 26:92–123
70. Saunders AD, Storey M, Kent RW, Norry MJ (1992) Consequences of plume lithosphere interactions. In: Storey BC, Alabaster J, Pnakhurst RJ (eds) Magmatism and the causes of continental break-up, vol 68. Geological Society of London Special Publications, London, pp 41–60
71. Pearce JA (2008) Geochemical fingerprinting of oceanic basalts with applications to ophiolite classification and the search for Archean oceanic crust. Lithos 100:14–48
72. Hanson GN (1978) The application of trace elements to the petrogenesis of igneous rocks of granitic composition. Earth Planet Sci Lett 38:26–43
73. Green DH, Ringwood AE (1968) Genesis of the calc-alkaline igneous rock suite. Contrib Miner Petrol 18:105–162
74. Green DH (1973) Experimental mantle studies on a model upper mantle composition under water-saturated and water-unsaturated conditions. Earth Planet Sci Lett 19:37–53
75. Lassiter JC, DePaolo DJ (1997) Plume/lithosphere interaction in the generation of continental and oceanic flood basalts|: chemical and isotope constraints. In: Mahoney J (ed) Large igneous provinces: continental, oceanic, and planetary flood volcanism. Geophysical Monography 100, American Geophysical Union, Washionton, DC, pp 335–355
76. Melluso L, Sethna SF (2011) Mineral compositions in the Deccan igneous rocks of India: an overview. In: Ray J, Sen G, Ghosh B (eds) Topics in igneous petrology. Springer, Heidelberg, pp 135–160

77. Kessel R, Schmidt MW, Ulmer P, Pettke T (2005) Trace element signature of subduction-zone fluids, melts and supercritical liquids at 120–180 km depth. Nature 437:724–727
78. Woodhead JD, Hergt JM, Davidson JP, Eggins SM (2001) Hafnium isotope evidence for 'conservative' element mobility during subduction zone processes. Earth Planet Sci Lett 192:331–346
79. McKenzie D, O'Nions RK (1991) Partial melt distribution from inversion of rare earth element concentrations. J Petrol 32:1021–1091
80. Aldanmaz E, Pearce JA, Thirlwall MF, Mitchell JG (2000) Petrogenetic evolution of late Cenozoic, post-collision volcanism in western Anatolia, Turkey. J Volcanol Geoth Res 102:67–95
81. Pearce JA, Harris NBW, Tindle AG (1984) Trace element discrimination diagrams for the tectonic interpretation of granitic rocks. J Petrol 25:956–983
82. Jung S, Masberg P, Mihm P, Hoernes H (2009) Partial melting of diverse crustal sources: constraints from Sr–Nd–O isotope compositions of quartz diorite-granodiorite leucogranite associations (Kaoko Belt, Namibia). Lithos 111:236–251
83. Li J, Niu Y, Hu Y, Chen S, Zhang Y, Duan M, Sun P (2016) Origin of the late early Cretaceous granodiorite and associated dioritic dikes in the Hongqilafu pluton, northwestern Tibetan Plateau: a case for crust-mantle interaction. Lithos 312:37–53
84. Defant MJ, Drummond MS (1990) Derivation of some modern arc magmas by melting of young subducted lithosphere. Nature 347:662–665
85. Castillo PR (2012) Adakite petrogenesis. Lithos 134:304–316
86. Akwinga VA, Basem Z, Bernd L, Dirk F, Ray B, Cheo ES (2014) Geochemistry and geochronology of the ~620 Ma gold-associated Batouri granitoids Cameroon. Int Geol Rev. https://doi.org/10.1080/00206814.2014.951003
87. Seo J, Choi S-G, Oh CW (2010) Petrology, geochemistry, and geochronology of the post-collisional Triassic mangerite and syenite in the Gwangcheon area, Hongseong Belt, South Korea. Gondwana Res 18:479–496
88. Murphy JB, Hynes AJ (1990) Tectonic control on the origin and orientation of igneous layering: an example from the Greendale Complex, Antigonish Highlands, Nova Scotia, Canada. Geology 18:403–406
89. Nkouandou OF, Bardintzeff JM, Dourwe DP, Fagny Mefire A (2016) Geochemistry and petrogenesis of mafic doleritic dykes at mbaoussi (Adamawa Plateau, Cameroon, Central Africa). J Geogr Environ Earth Sci Int 8(1):1–18
90. Tchaptchet Tchato D, Simeni Wambo NA, Keutchafo Kouamo NA, Tchouankoue JP, Cucciniello C (2017) Geology, mineralogy and geochemistry of the Kekem dyke swarm (Western Cameroon): insights into Paleozoic-Mesozoic magmatism and geodynamic implications. C R Geosci 349:175–185
91. Gibson SA, Thompson RN, Day JA (2006) Time scales and mechanisms of plume-lithosphere interactions: 40Ar/39Ar geochronology and geochemistry of alkaline igneous rocks from Parana–Etendenka large igneous province. Earth Planet Sci Lett 251:1–17
92. Kuepouo G, Tchouankoue JP, Nagao T, Sato H (2006) Transitional tholeiitic basalts in the Tertiary Bana volcano-plutonic complex. Cameroon Line J Afr Earth Sci 45:318–332
93. Youbi N, Martins LT, Manuel JM, Ibouh H, Madeira J, Ait Chayeb EHA, Boukhari AE (2003) The central Atlantic magmatic province: insight from fragments of Pangea. Geophys I Monogr Ser 136:179–207
94. Tchaptchet Tchato D, Schulz B, Nzenti JP (2009) Electron microprobe dating and thermobarometry of Neoproterozoic metamorphic events in the Kekem area, Central African Fold Belt of Cameroon. Neues Jahbur Min Abh 186(1):95–109
95. Noutchogwe TC, Koumetio F, Manguelle-Dicoum E (2010) Structural features of South Adamawa (Cameroon) inferred from magnetic anomalies: hydrogeological implications. C R Geosci 342:467–474
96. Dadd KA, Kellerson L, Borissova I, Nelson G (2015) Multiple sources for volcanic rocks dredged from the western Australian rifted margin. Mar Geol 368:42–57